-RESEARCH PAPER-

International Journal of Mining and Geo-Engineering

IJMGE

IJMGE 60-1 (2026) 9-15

DOI: 10.22059/IJMGE.2026.399972.595285

Cross gradient based joint inversion of EM-LIN and DC resistivity data

Ramin Varfinezhad [a,*] and Mohammad Ferasat [b]

[a] *Institute of Geophysics, University of Tehran, Tehran, Iran.*

[b] *Department of Engineering Geology, School of Geology, College of science, University of Tehran, Tehran, Iran.*

Article History:

Received: 03 August 2025.

Revised: 20 September 2025.

Accepted: 02 March 2026.

ABSTRACT

Non-uniqueness and instability of single geophysical approaches may be reduced by utilizing constraints and a priori information in terms of regularization, but deriving enough information about subsurface sources generally demands integration of two or more geophysical data sets. Cross gradient based joint inversion is one of the most widespread ways of geophysical data integration where involved methods share their information for each other through cross gradient function. In this paper, the joint inversion of DC resistivity and EM34 data was applied to the measured data at Morgenzon Farm site in South Africa, where the reconstruction of a dolerite dyke or sill is the principal target indicating the presence of groundwater. The separate inversion of DC resistivity data highlights a two layered medium as an interface and a small weak anomaly in the middle of the profile, while EM34 inverse model indicates a resistive dyke in the middle of the profile with a depth range from 5 to 15 m. Join inversion allows the involving methods to propagate their characteristics to each other, and it was found that joint inverse model of the DC resistivity is the best result to reconstruct the subsurface structure. In addition, joint inversion results were compared with the cooperative inversion of these approaches. Ultimately, the measured magnetic and gravity data were also inverted, allowing their joint interpretation with the separate and joint resistivity models.

Keywords: *Cross gradient constraint, DC resistivity, EM-LIN, Dolerite dyke.*

1. Introduction

Quantitative interpretation of geophysical methods is usually carried out by inverse modeling. However, for both gravity and magnetic data, imaging methods are also widespread [1-5]. In addition, processing of seismic data can be mostly as helpful as inverse modeling [6-8], but inversion is necessary for DC resistivity and Electromagnetic (EM) data interpretation. Inversion of geophysical data suffers about two main problems: non-uniqueness, and instability of inverse model. Besides, interpretation based on a single data cannot lead to promising results about the subsurface structure [9, 10]. Therefore, integration of geophysical data seems to be mandatory and logical strategy.

Geophysical data sets may be combined utilizing three approaches: I) joint interpretation for which separate inversions of available data sets are first executed, then interpretation is made based on these inverse models, geological data and any other available information [11, 12], II) sequential or cooperative inversion where inversion of one geophysical data set is used as an initial model for another method [13, 14], and III) joint inversion that can be made based on petrophysical constraints [15, 16] and structural similarities [17, 18].

DC resistivity is extensively implemented for diverse geological targets such as mineral exploration [19, 20] environmental and engineering investigations [21, 22, 23], hydrological surveys [24], and archeological prospecting [25, 26, 27]. Electromagnetic at low induction number (EM-LIN) method has important features like low cost, high speed for data collection and being non-destructive which made it popular to be manipulated for different subsurface anomalies [28-32]. EM-LIN consists of three techniques: EM31, EM38 and EM34 which is the case here. Detailed information about their discrepancies may be found in Parnow et al, (2021). Integration of EM-LIN and DC resistivity data have been manipulated as joint interpretation [33-36] but their joint inversion has never been investigated.

A cross-gradient joint inversion of DC resistivity and EM-LIN is performed, and it is evaluated against cooperative and individual inversions at the Morgenzon Farm site. In addition, joint inversion results are compared with cooperative inversion of the involved approaches. Finally, single inversion results of gravity and magnetic data sets will be also obtained to allow a joint interpretation procedure for this case study. Considering this issue that all types of geophysical data integration are implemented for a given real case (here, Morgenzon Farm site) makes this research more unique.

2. Methodology

In this section, forward problems of both methods are introduced, which are Fredholm integral equations of the first kind. Then, an individual inversion algorithm is presented for both methods based on the damped weighted minimum length solution [20, 29] Ultimately, the joint inverse modeling based on cross-gradient constraint is presented.

2.1. Forward problems of DC resistivity and EM-LIN methods

On the premise of Born approximation, linear integral equations were introduced for DC resistivity and EM-LIN methods by Perez-Flores et al [36]. These integral equations may be classified as Fredholm integral equations of the first kind with 2D general form as [37]:

* Corresponding author. *Tel:* +98 21 82885016, *E-mail address:* : ramin.varfi@ut.ac.ir (R. Varfinezhad).

$$d(s) = \iint G(s,x,z)m(x,z)dxdz \quad (1)$$

where, (s) refers to measured data (log10 of apparent resistivities for DC resistivity and apparent conductivities for EM-LIN), $G(s,x,z)$ is kernel function that depends on the geometry of configurations that are used during data collection for both methods, and $m(x,z)$ is subsurface model expressing log10(resistivity)/conductivity distribution. Appropriate formulas of kernel functions for DC resistivity and EM-LIN may be found in literature [36]. Equation (1) must be discretized to allow numerical modeling; therefore, the subsurface is divided into a lot of prisms with infinite length along one direction (say, *y*), and the midpoint rule technique is manipulated for discretization of equation (1) [20]. As a consequence, the previous equation may be written as the following matrix equation:

$$\mathbf{d} = \mathbf{Gm} \quad (2)$$

where**,** $\mathbf{d}$ and $\mathbf{m}$ are respectively data and model vectors, and $\mathbf{G}$ is forward operator. Detailed descriptions of 2D modeling for DC resistivity and EM-LIN techniques can be found in Perez-Flores et. al [36].

2.2. Separate inversion algorithm

Ambiguity and instability of geophysical inverse problems need a priori information and constraints that may be inserted in the inverse procedure through regularization. Tikhonov and Arsenin [38] proposed the following general formula as an objective function:

$$\min \rightarrow \|\boldsymbol{W_d}(\boldsymbol{Gm} - \boldsymbol{d})\|_2^2 + \boldsymbol{\alpha}\|\boldsymbol{W_m}(\boldsymbol{m} - \boldsymbol{m_0})\|_2^2 \quad (3)$$

where the first term describes data misfit weighted by the data covariance matrix $\boldsymbol{W_d}$, and the second term denotes the model objective function, which is weighted by the model weighting matrix $\boldsymbol{W_m}$. $\boldsymbol{m_0}$ expresses initial model and may be constructed using a priori information such as a geology model, an inverse model of other geophysical methods, and etc. Degree of the second term contribution in the inverse model is determined by the regularization parameter α. Large values for α increase the bias introduced in the inverse model and consequently model resolution is reduced; therefore, RMS error of data misfit is augmented. Different algorithms have been suggested for individual inversion of DC resistivity and EM-LIN data in the last decades [28, 36, 39-43], but we utilize the damped weighted minimum length solution algorithm for DC resistivity and EM-LIN data introduced respectively by Varfinezhad et al, [20] and Parnow et al, [27]:

$$\boldsymbol{m} = \boldsymbol{m}_0 + (\boldsymbol{W_m^{-1}G^T})(\boldsymbol{GW_m^{-1}G^T} + \alpha\boldsymbol{W_d})^{-1}(\boldsymbol{d} - \boldsymbol{Gm}_0) \quad (4)$$

$\boldsymbol{W_m}$ is assumed to be a depth weighting function, which was pioneered by Li and Oldenburg for potential methods ([44, 45]. Since then, depth weighting has been widely used in potential field data inverse algorithms [11, 46-48]. For the first time, Varfinezhad et al, [9] used depth weighting for DC resistivity inversion and its joint inversion with the magnetometry method, while extensive investigation of this constraint in DC resistivity data inversion was carried out by Varfinezhad et al, [20]. Parnow et al, [27] manipulated depth weighting as an exponential function of depth for EM-LIN data. In this paper, the same function proposed by Li and Oldenburg [44, 45] is used, but the exponent of depth weighting is adopted to be 1 as the default value for both approaches.

2.3. Joint inversion using cross-gradient

According to the joint inversion algorithm presented by Gallardo and Meju [49], a joint inverse algorithm for DC resistivity and EM-LIN data sets may be developed. The 2D form of the cross-gradient function associated with involving approaches is expressed as:

$$t = \nabla m_R(x,z) \times \nabla m_E(x,z) \quad (5)$$

where $m_R(x,z)$ and $m_E(x,z)$ stand respectively for resistivity and conductivity models. Expanding equation (5) results in the following formula:

$$t(x,z) = \left(\frac{\partial m_R(x,z)}{\partial z}\right)\left(\frac{\partial m_E(x,z)}{\partial x}\right) - \left(\frac{\partial m_R(x,z)}{\partial x}\right)\left(\frac{\partial m_E(x,z)}{\partial z}\right) \quad (6)$$

Discretizing the previous equation by finite difference numerical technique leads to equation (7):

$$t \cong \frac{4}{\Delta x \Delta z}\left(m_{Rc}(m_{Eb} - m_{Er}) + m_{Rr}(m_{Ec} - m_{Eb}) + m_{Rb}(m_{Er} - m_{Ec})\right) \quad (7)$$

According to this formula, for a given cell (identified by subscript *c*), subscripts *b* and *r* denote, respectively, the bottom and right closer cells. For the joint process, the objective function defined in equation (8) is minimized under cross-gradient constraint [49]:

$$\min\left\{\varphi(m_R, m_G) = \left\|\begin{matrix} d_R - A_R m_R \\ d_E - A_E m_G \end{matrix}\right\|^2_{C_{dd}^{-1}} + \left\|\begin{matrix} \alpha_R W_{mR} m_R \\ \alpha_E W_{mE} m_E \end{matrix}\right\|^2 + \left\|\begin{matrix} m_R - m_{0R} \\ m_E - m_{0E} \end{matrix}\right\|^2_{C_{RR}^{-1}}\right\} \quad (8)$$

subject to $t(m_R, m_E) = 0$.

where d_R and d_E stand for the log10 of measured apparent resistivities and measured apparent conductivities, respectively. A_R and A_E denote forward operator matrices corresponding with resistivity and EM-LIN methods, C_{dd} refers to the data covariance matrix assumed to be a diagonal matrix. $m = [m_R; m_E]^T$ expresses the vector of model parameters, m_{0R} and m_{0E} are initial models associated with the both approaches where covariance matrix is C_{RR}^{-1} and $t(m_R, m_E)$ defines cross-gradient values for all model cells. α_R and α_E refer to regularization parameters of both methods and W_{mR} and W_{mE}, called model weighting matrices, are depth weighting functions associated with DC resistivity and EM-LIN. Gallardo and Meju [49] found the following solution for the objective function in equation (8), using the Lagrangian multipliers technique:

$$m = N_1^{-1}n_2 - N_1^{-1}B^T(BN_1^{-1}B^T)^{-1}(BN_1^{-1}n_2 - Bm_0 + t_0) \quad (9)$$

where:

$$N_1 = \begin{bmatrix} A_R^T A_R + \alpha_R^2 W_{mR} & 0 \\ 0 & A_E^T A_E + \alpha_E^2 W_{mE} \end{bmatrix} \quad (10)$$

And:

$$n_2 = \begin{bmatrix} A_R^T\{d_R - A_R m_{0R}\} \\ A_E^T\{d_E - A_E m_{0E}\} \end{bmatrix} \quad (11)$$

B is the jacobian matrix of the cross-gradient function t, t_0 is the cross-gradient function of resistivity and conductivity initial models. The right side of equation (9) is composed of two terms: the first term expresses separate inversions of both methods, and the second one describes the effect of each model shared for another one through cross-gradient constraint. The combination of these terms provides a joint inversion solution.

3. Geology

Morgenzon Farm site is one of the sites of Karoo Supergroup (Figure 1), which is the most well-known stratigraphy in South Africa [50]. The Karoo Supergroup is made up of a thick succession of dominantly sedimentary strata that were deposited during 310-182 million years ago [51]. These strata consist of sedimentary rocks which are expressed as rocks that have shaped at or close to the Earth's surface through the deposition and solidification of sediments, especially sediments carried by water (e.g. rivers, lakes, and oceans), ice (glaciers) and wind [34].

Karoo Supergroup sediments are classified into groups explained as accumulation of two or more formations that share certain lithological characteristics [34]. These groups are named: Dwyka, Ecca, Beaufort, Stormberg and Drakensberg Groups [52]. The group names were adopted according to the changes in tectonic and climatic conditions throughout the time of deposition in the Karoo Supergroup, giving rise to the sequence across the Karoo Basin. Fracturing of Karoo rocks is the consequence of two main factors: 1) rife volcanism throughout the Jurassic era, and 2) intrusion of dolerite laccoliths, sills and dykes which had a great contribution.

Dolerite dyke and sill structures are usually the most important target for groundwater surveys in the Karoo [53]. Due to the large resistivity

contrasts of dolerite structures with sedimentary background, application of resistivity-based methods such as DC resistivity and EM34 can be useful to detect them. Furthermore, dolerite susceptibility has a significant discrepancy with the susceptibility of its encompassing rocks. Hence, as will be shown in the ***Discussion*** section, magnetometry may also be practical to detect dolerite structures.

4. Inversion results and interpretation

4.1. Joint inversion results of EM-LIN and DC resistivity

EM34 data were collected by HMD configuration with data spacing of 10 m and T-R separation of 20 m along a profile which its length is 400m. Apparent resistivity data were collected by Wenner-Schlumberger array with unit electrode spacings of 5 and 10 m, where the number of data was 900. Measured data sets for both approaches are displayed in Figure 2.

Cross gradient joint inversion models of DC resistivity and EM-LIN (using HMD) are displayed in Figure 3. It should be mentioned that we show both individual and joint models of the EM-LIN approach in terms of resistivity for simplicity, but all EM-LIN computations are accomplished in the conductivity domain. The EM-LIN joint model doesn't improve significantly because the layered medium is not recovered after the joint process and only some improvements may be observed in the deep and middle parts of the profile. Conversely, the DC resistivity joint model improves significantly since dyke is retrieved after the joint inversion process and this model is more consistent with real subsurface. First, these observations mathematically are explained, then joint models are compared with cooperative results: I) **region 1**: the gradient of resistivities in the EM-LIN section is large and the gradient of resistivities in the DC resistivity section is also considerable. Therefore, EM-LIN can help DC resistivity to reconstruct dyke very well, II) **region 2:** the gradient of resistivities in the EM-LIN section is really small, while for DC resistivity is large, so DC resistivity may be useful to improve the EM-LIN model somewhat in this region, III) **regions 3**: the gradient of the EM-LIN model is very small and the gradient of DC resistivity model is really lower than region 2. Therefore, we cannot see even small improvement in the EM-LIN model after the joint process. RMS misfit errors of separate and joint inversion procedures are presented in Table 1, stating that RMS misfit errors after joint inversion are larger than separate inversion. Why? It should be noted that the joint inversion process includes an additional constraint (the cross-gradient function) which is equivalent to the more bias (in spite of improvement in model recovery, especially for the DC resistivity joint inversion model) and, consequently, can lead to larger RMS misfit error.

4.2. Simultaneous separate and cooperative inversions

Separate and cooperative inversions for HMD and DC resistivity data sets, during a simultaneous procedure, may be observed in Figure 4. A separate inversion of the EM34 technique reconstructs a relatively thick dyke extended horizontally from about 180 to 200 m, while its depth range is from less than 5 to about 15 m. Separate inversion of measured apparent resistivities recovers an interface model with a fluctuating boundary which is extended to the near surface in the middle of the profile. It should be noted that a very small and thin anomaly may also be found in the middle of the profile with a depth range of 5 to 10 m. Cooperative resistivity model for EM34 constrained by the DC resistivity method, shows an interface model with a resistive dyke in the middle of the profile, but dyke is not resolved, as well as separate inversion of EM34 data. In other words, the interface zone which could not be retrieved just by EM34 data, due to the exploration depth limitation of the HMD configuration using a T-R distance of 20 m, is revealed in the cooperative section, but the dyke zone is spoiled. Conversely, the cooperative inverse section of DC resistivity demonstrates both interface and dyke zones with good resolution. Actually, this model shows enough improvement with respect to individual inversion results. The cooperative inverse process applied to the real case includes the following main conclusions:

I) The EM34 cooperative inverse model utilized inversion of DC resistivity data as the initial model. Therefore, it is biased toward individual inversion of DC resistivity approach through cooperative inversion that had two different consequences: the first one was the presence of an interface zone which was the good side of story (advantage) and, the second one was dyke destruction comparing with individual inversion (disadvantage).

II) DC resistivity approximately took advantage of the cooperative inverse procedure so that the interface zone was preserved, and the dyke zone was recovered. Generally speaking, cooperative inversion is really superior to the separate inversion for the DC resistivity approach.

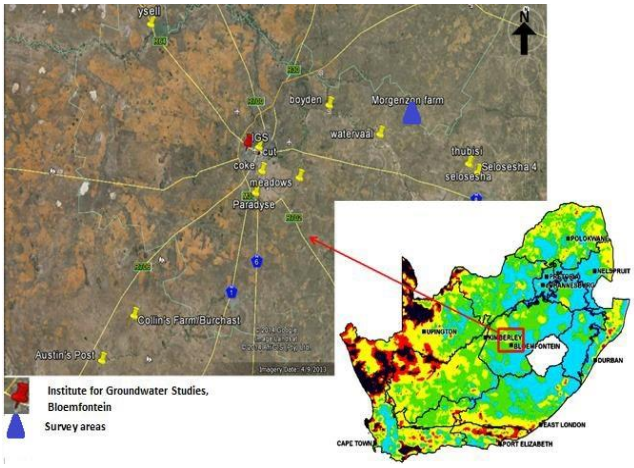

Figure 1. Map which displays the study area [34].

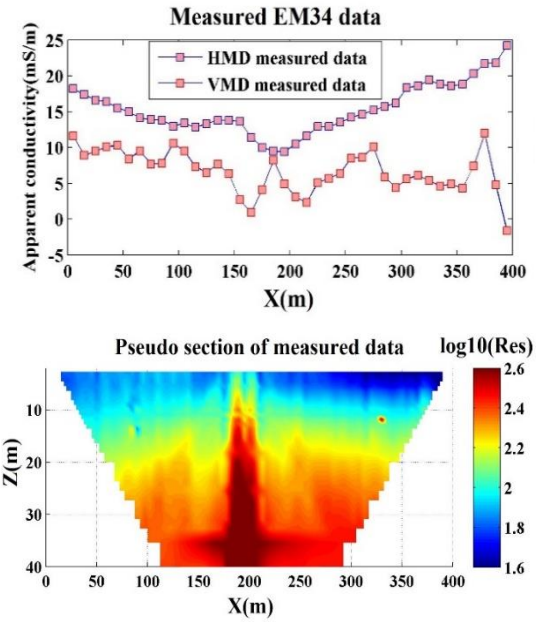

Figure 2. Measured data of both EM34 (left) and DC resistivity (right) approaches.

5. Discussion

In addition to the measured DC resistivity and EM34 data sets, magnetometry and gravity data are also collected along the same profile. Sample intervals of magnetic data are not equal, but all of them are less than 2 m, and the number of data is 245. Gravity data have the sample

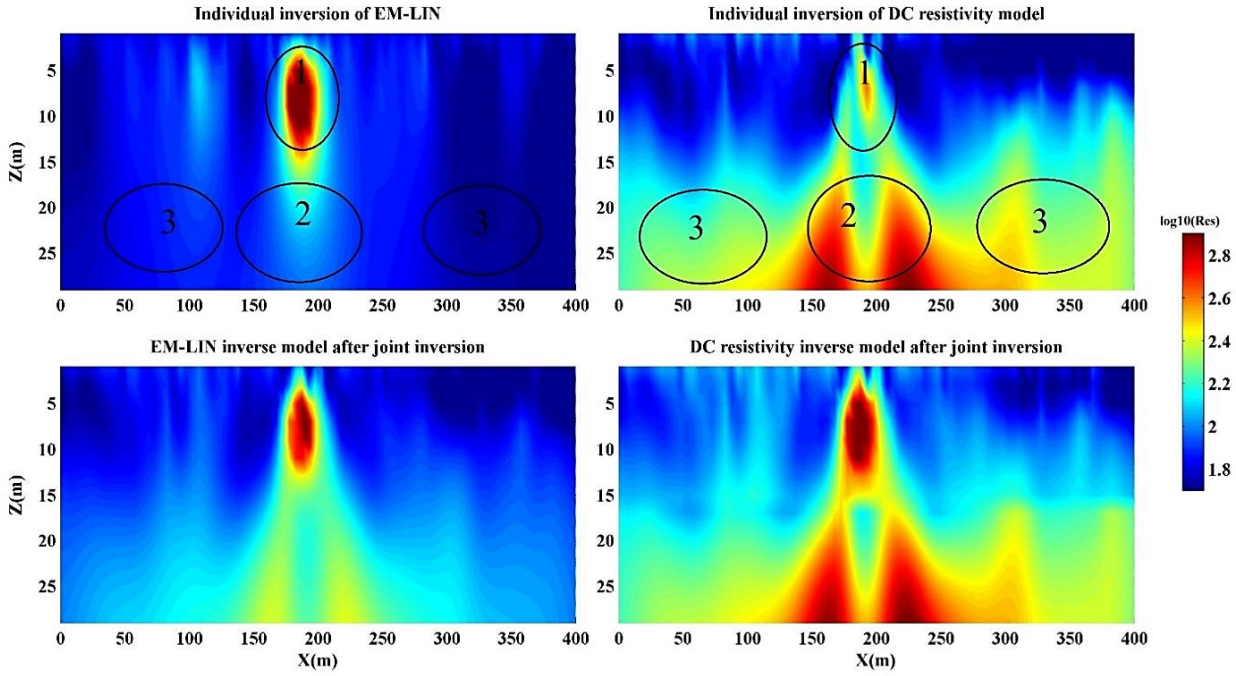

Figure 3. Individual and joint inversion models of EM-LIN and DC resistivity approaches.

Table 1. RMS misfit errors of computed data for joint inversions of EM34 and DC resistivity approaches.

Calculated data	RMS error (%)
Calculated data from separate resistivity inversion	2.37
Calculated data from joint resistivity inversion	3.88
Calculated data from separate HMD inversion	2.21
Calculated data from joint HMD inversion	3.76

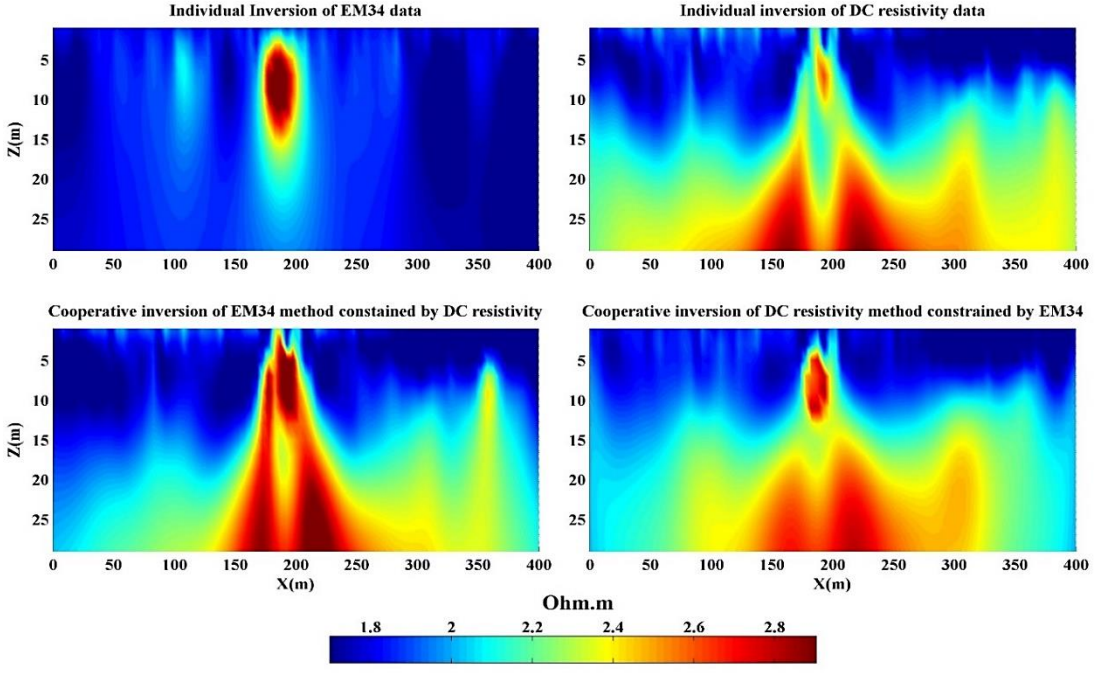

Figure 4. Separate and cooperative inversion models for both EM34 using HMD and DC resistivity data sets.

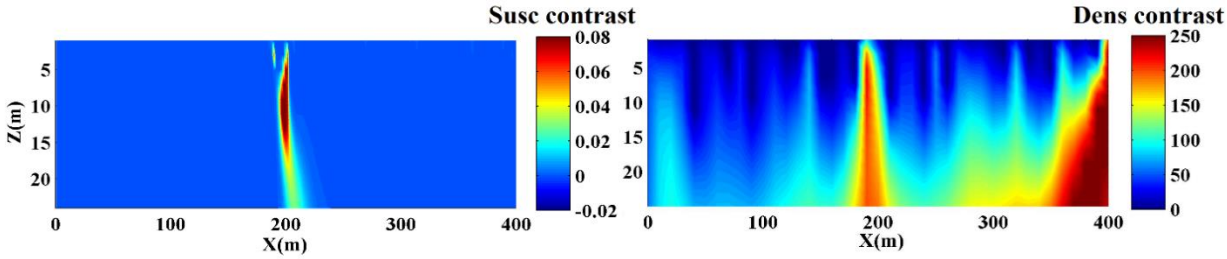

Figure 5. Reconstructed models of susceptibility and density contrasts from measured magnetic and gravity data.

interval of 10 m, and the number of data is 40. Inversion models derived from both magnetometry and gravity measurements are displayed in Figure 5. The damped weighted minimum length solution was used for the inversion of both data sets [11, 48].

Susceptibility contrast distribution is demonstrative of a thin dyke in the middle of the profile extending approximately from 190 to 200 m with a depth range from near surface to more than 15 m. This result is in good agreement with EM34 inversion models; however, recovered dyke from magnetic data is thinner. Furthermore, the magnetic model, like EM34 and in contrast to DC resistivity, cannot sense the layered feature of the subsurface. Therefore, magnetometry can also act like a constraint for successful integration with DC resistivity in terms of joint inversion or cooperative inversion.

The inversion model derived from gravity data shows a relatively layered model including a thin dyke in the middle of the profile, which is somewhat consistent with cooperative inversion models. However, the depth of the boundary between layers and the depth range of the dolerite dyke have a relatively significant difference with the cooperative inversion model of DC resistivity.

On aggregate, joint interpretation of EM34, DC resistivity, and magnetometry methods provides enough confidence about the presence of a resistive/magnetized dyke in the middle of the profile with the depth range from less than 5 to 15m, which is the principal target for groundwater presence in the area. The presence of a two-layered medium (as an interface) may also be deduced from even the pseudo-section of the measured apparent resistivities. Furthermore, we observe practically the importance and usefulness of different available measurements, which result in promising insight about subsurface structure in terms of cooperative inversion and joint interpretation.

6. Conclusion

Ann algorithm for simultaneous individual and cooperative inversions of DC resistivity and EM34 methods was introduced, and applied it to the real data collected at Morgenzon Farm in South Africa to detect subsurface structure with emphasis on a dolerite dyke as an indicator for the presence of groundwater in the area. The regularized weighted minimum length solution algorithm was used for the individual inversion of both methods. During an iterative joint inversion process, the inverse output of each method was shared for another one through the cross-gradient function. Comparing separate and joint models clearly indicated that the DC resistivity joint inverse model was the best result. Individual inversion of DC resistivity detected a two-layered medium including a very small resistive anomaly in the first layer, but the EM34 inverse model showed a relatively thick anomaly in the middle of the profile, indicating a resistive dolerite dyke. Cooperative inversions of EM34 (for HMD configuration) and DC resistivity were also implemented, and the cooperative DC resistivity model was really promising about the recovery of subsurface structure.

In addition to the joint inversion, a brief joint interpretation was made from resistivity models and the inverse models obtained from magnetic and gravity data sets. The susceptibility model retrieved a relatively thin dyke in the middle of the profile, which was really in good correspondence with EM34 inverse sections. Inversion of gravity data produced density model that was consistent with resistivity joint inversion and susceptibility models.

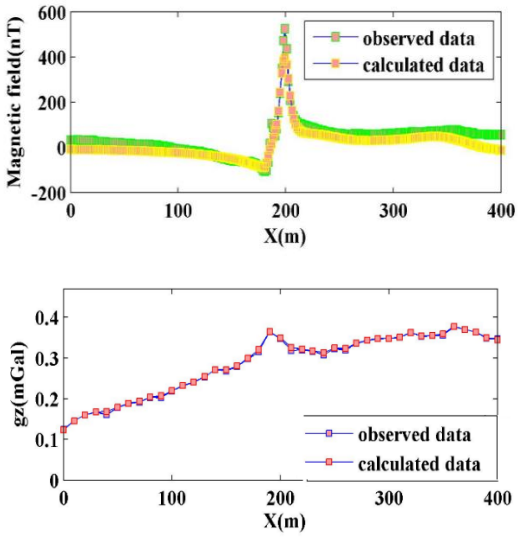

Figure 6. Calculated data from inverse models shown in figure 5 versus measured data for both magnetic and gravity methods.

References

[1]. Pilkington, M. (1997). 3-D magnetic imaging using conjugate gradients. *Geophysics*, *62*(4), 1132-1142.

[2]. Fedi, M., Hansen, P. C., & Paoletti, V. (2005). Analysis of depth resolution in potential field inversion: a tutorial. *Geophysics*, *70*, A1-A11.

[3]. Fedi, M. (2007). DEXP: A fast method to determine the depth and the structural index of potential fields sources. *Geophysics*, *72* (1), I1-I11.

[4]. Fedi, M., & Pilkington, M. (2012). Understanding imaging methods for potential field data. *Geophysics*, *77*(1), G13-G24.

[5]. Baniamerian, J., Oskooi, B., & Fedi, M. (2017). Source imaging of potential fields through a matrix space-domain algorithm. *Journal of Applied Geophysics*, *136*, 51-60.

[6]. Wang, H., Li, M., & Shang, X. (2016). Current developments on micro-seismic data processing. *Journal of Natural Gas Science and Engineering*, *32*, 521-537.

[7]. Koteleva, N., & Frenkel, I. (2021). Digital processing of seismic data from open-pit mining blasts. *Applied Sciences*, *11*(1), 383.

[8]. Mousa, W. A., & Al-Shuhail, A. A. (2022). *Processing of seismic reflection data using MATLAB*. Springer Nature.

[9]. Varfinezhad, R., Oskooi, B., & Fedi, M. (2020). Joint inversion of DC resistivity and magnetic data, constrained by cross gradients, compactness and depth weighting. *Pure and Applied Geophysics*, *177*, 4325-4343.

[10]. Najaftomraei, M., Moghadam, S., Varfinezhad, R., Goudarzi, A., & Faghih, A. (2024). Subsurface characterization in southeastern Asaluyeh using DC resistivity and ground penetrating radar. *International Journal of Mining and Geo-Engineering*, *58* (4), 423-429.

[11]. Milano, M., Varfinezhad, R., Bizhani, H., Moghadasi, M., Kalateh, A. N., & Baghzendani, H. (2021). Joint interpretation of magnetic and gravity data at the Golgohar mine in Iran. *Journal of Applied Geophysics*, *195*, 104476.

[12]. Ghari, H., Varfinezhad, R., & Parnow, S. (2023). 3D joint interpretation of potential field, geology, and well data to evaluate a salt dome in the Qarah-Aghaje area, Zanjan, NW Iran. *Near Surface Geophysics*, *21* (3), 233-246.

[13]. Singh, A., Mishra, PK, & Sharma, S.P. (2019). 2D cooperative inversion of direct current resistivity and gravity data: A case study of uranium bearing target rock. *Geophysical Prospecting*, *67* (3), 696-708.

[14]. Varfinezhad, R., Parnow, S., Florio, G., Fedi, M., & Mohammadi Vizheh, M. (2023). DC resistivity inversion constrained by magnetic method through sequential inversion. *Acta Geophysica*, *71* (1), 247-260.

[15]. Ghose, R., & Slob, E.C. (2006). Quantitative integration of seismic and GPR reflections to derive unique estimates for water saturation and porosity in subsoil. *Geophysical Research Letters*, *33* (5).

[16]. Varfinezhad, R., Hafizi, M. K., & Hashemi, H. (2016). Application of different inverse methods for combination of vS and vGPR data to estimate porosity and water saturation. *Journal of the Earth and Space Physics*, *41*(4), 89-94.

[17]. Haber, E., & Oldenburg, D. (1997). Joint inversion: a structural approach. *Inverse problems*, *13*(1), 63.

[18]. Gallardo, L. A., & Meju, M. A. (2011). Structure-coupled multiphysics imaging in geophysical sciences. *Reviews of Geophysics*, *49*(1).

[19]. Legault, J.M., Carriere, D., & Petrie, L. (2008). Synthetic model testing and distributed acquisition dc resistivity results over an unconformity uranium target from the Athabasca Basin, northern Saskatchewan. *The Leading Edge*, *27* (1), 46-51.

[20]. Varfinezhad, R., Ghari, H. and Rafiei, R., 2022. Topography incorporated inversion of DC resistivity data using integral equation vs. Res2dinv software. Bulletin of Geophysics & Oceanography (BGO), 63 (3).

[21]. Chambers, JE, Kuras, O, Meldrum, PI, Ogilvy, RD, & Hollands, J (2006). Electrical resistivity tomography applied to geologic, hydrogeologic, and engineering investigations at a former waste-disposal site. *Geophysics*, *71* (6), B231-B239.

[22]. Rucker, DF, Loke, MH, Levitt, MT, & Noonan, GE (2010). Electrical-resistivity characterization of an industrial site using long electrodes. *Geophysics*, *75*(4), WA95-WA104.

[23]. Ghari, H., Parnow, S., Varfinezhad, R., Milano, M., Fourie, F.D. and Tosti, F., 2024. Cross-Gradient Joint Inversion of DC Resistivity and Gravity Gradient Data: A Multi-Disciplinary Approach for Geoscience, Heritage, and the Built Environment. Remote Sensing, 16 (23), p.4468.

[24]. Wilson, S. R., Ingham, M., & McConchie, J. A. (2006). The applicability of earth resistivity methods for saline interface definition. *Journal of hydrology*, *316* (1-4), 301-312.

[25]. Tsokas, G.N., Tsourlos, P.I., Vargemezis, G., & Novack, M. (2008). Non-destructive electrical resistivity tomography for indoor investigation: the case of Kapnikarea Church in Athens. *Archaeological prospection*, *15* (1), 47-61.

[26]. Varfinezhad, R., & Oskooi, B. (2020). 2D DC resistivity forward modeling based on the integral equation method and a comparison with the RES2DMOD results. *Journal of the Earth and Space Physics*, *45* (4), 43.

[27]. Parnow, S., Oskooi, B., & Florio, G. (2021). Improved linear inversion of low induction number electromagnetic data. *Geophysical Journal International*, *224* (3), 1505-1522.

[28]. Pérez-Flores, M. A., Antonio-Carpio, R. G., Gómez-Treviño, E., Ferguson, I., & Méndez-Delgado, S. (2012). Imaging of 3D electromagnetic data at low-induction numbers. *Geophysics*, *77* (4), WB47-WB57.

[29]. Parnow, S., Oskooi, B., & Florio, G. (2021). Improved linear inversion of low induction number electromagnetic data. *Geophysical Journal International*, *224* (3), 1505-1522.

[30]. Varfinezhad, R., & Parnow, S. (2022). 3D Electromagnetic low induction number modeling using integral equations. *Journal of the Earth and Space Physics*, *47* (4), 99-110.

[31]. Ghari, H. and Varfinezhad, R., 2022. 2D Linear inversion of ground-based controlled-source electromagnetic data under a low induction number condition.

[32]. Ghari, H. and Mahdavi, M., 2024. Dyke detection as the main target of groundwater exploration using Magnetometry and Electromagnetic data. International Journal of Mining and Geo-Engineering, 58 (3), pp.257-262.

[34]. Makhokha, D., & Fourie, F. (2016). *A systematic approach to the interpretation of conductivity anomalies across intrusive dolerite dykes and sills in the Karoo Supergroup* (Doctoral dissertation, MSc thesis. University of the Free State, Bloemfontein).

[35]. Ghari, H., 2025. Joint Interpretation of Electromagnetic in Low Induction Number and Electrical Resistivity Tomography: A Case Study on Data from an Area in South Africa. Journal of Analytical and Numerical Methods in Mining Engineering, 15(42), pp.15-23.

[36]. Pérez-Flores, M. A., Méndez-Delgado, S., & Gómez-Treviño, E. (2001). Imaging low-frequency and dc electromagnetic fields using a simple linear approximation. *Geophysics*, *66*(4), 1067-1081.

[37]. Aster, R. C., Borchers, B., & Thurber, C. H. (2018). *Parameter estimation and inverse problems*. Elsevier.

[38]. Tikhonov, AN, & Arsenin, VIAK (1977). Solutions of ill-posed problems.

[39]. Li, Y., & Oldenburg, D. W. (1992). Approximate inverse mappings in DC resistivity problems. *Geophysical Journal International*, *109* (2), 343-362.

[40]. Loke, M.H., & Barker, R.D. (1996). Rapid least-squares inversion of apparent resistivity pseudo-sections by a quasi-Newton method1. *Geophysical prospecting*, *44* (1), 131-152.

[41]. Auken, E., & Christiansen, A. V. (2004). Layered and laterally constrained 2D inversion of resistivity data. *Geophysics*, *69*(3), 752-761.

[42]. Günther, T., Rücker, C., & Spitzer, K. (2006). Three-dimensional modeling and inversion of DC resistivity data incorporating topography—II. Inversion. *Geophysical Journal International*, *166* (2), 506-517.

[43]. Gündoğdu, N. Y., & Candansayar, M. E. (2018). Three-dimensional regularized inversion of DC resistivity data with different stabilizing functionals. *Geophysics*, *83* (6), E399-E407.

[44]. Li, Y., & Oldenburg, D. W. (1996). 3-D inversion of magnetic data. *Geophysics*, *61* (2), 394-408.

[45]. Li, Y., & Oldenburg, D. W. (1998). 3-D inversion of gravity data. *Geophysics*, *63* (1), 109-119.

[46]. Boulanger, O., & Chouteau, M. (2001). Constraints in 3D gravity inversion. *Geophysical prospecting*, *49* (2), 265-280.

[47]. Cella, F., & Fedi, M. (2012). Inversion of potential field data using the structural index as weighting function rate decay. *Geophysical Prospecting*, *60* (2), 313-336.

[48]. Ghari, H., Varfinezhad, R., & Parnow, S. (2023). 3D joint interpretation of potential field, geology, and well data to evaluate a salt dome in the Qarah-Aghaje area, Zanjan, NW Iran. *Near Surface Geophysics*, *21* (3), 233-246.

[49]. Gallardo, L. A., & Meju, M. A. (2004). Joint two-dimensional DC resistivity and seismic travel time inversion with cross-gradients constraints. *Journal of Geophysical Research: Solid Earth*, *109* (B3).

[50]. Rubidge, T. M., 2005. The story of earth and life. 1st ed. Cape Town: struik Nature.

[51]. McCathy, T., & Rubidge, B. (2005). the Story of Earth and Life, a South African Perspective on a 4.6-billion-year Journey. *Struik, Cape Town, South Africa*, 184-211.

[52]. Geel, C., 2014. Brief geologic overview of the Cape Fold Belt and Karoo Basin: Field excursion to Matjiesfontein, 10th Inkaba yeAfrica conference. Matjiesfontein, Inkba yeAfrica.

[53]. Murray, R., Baker, K., Ravenscroft, P., Musekiwa, C., & Dennis, R. (2012). A groundwater-planning toolkit for the main Karoo basin: Identifying and quantifying groundwater-development options incorporating the concept of wellfield yields and aquifer firm yields. *Water SA*, *38* (3), 407-416. [1].